Atom Indonesia Vol. 39 No. 2 (2013) 65 - 74

Non-destructive Residual Stress Analysis Around The Weld-Joint of Fuel Cladding Materials of ZrNbMoGe Alloys

Parikin*, Bandriyana, I. Wahyono and A.H. Ismoyo
Center for Technology of Nuclear Industry Materials, National Nuclear Energy Agency
Puspiptek Area Serpong, Tangerang 15314, Indonesia

ARTICLE INFO

Article history:
Received 16 January 2013
Received in revised form 25 April 2013
Accepted 10 June 2013

Keywords:
ZrNbMoGe alloy
welding
residual stresses
X-ray diffraction

ABSTRACT

The residual stress measurements around weld-joint of ZrNbMoGe alloy have been carried out by using X-ray diffraction technique in PTBIN-BATAN. The research was performed to investigate the structure of a cladding material with high temperature corrosion resistance and good weldability. The equivalent composition of the specimens (in %wt.) was 97.5%Zr1%Nb1%Mo½%Ge. Welding was carried out by using TIG (tungsten inert gas) technique that completed butt-joint with a current 20 amperes. Three region tests were taken in specimen while diffraction scanning, While diffraction scanning, tests were performed on three regions, i.e., the weldcore, the heat-affected zone (HAZ) and the base metal. The reference region was determined at the base metal to be compared with other regions of the specimen, in obtaining refinement structure parameters. Base metal, HAZ and weldcore were diffracted by X-ray, and lattice strain changes were calculated by using Rietveld analysis program. The results show that while the quantity of minor phases tend to increase in the direction from the base metal to the HAZ and to the weldcore, the quantity of the ZrGe phase in the HAZ is less than the quantity of the ZrMo2 phase due to tGe element evaporation. The residual stress behavior in the material shows that minor phases, i.e., Zr_3Ge and $ZrMo_2$, are more dominant than the Zr matrix. The Zr_3Ge and $ZrMo_2$ experienced sharp straining, while the Zr phase was weak-lined from HAZ to weldcore. The hydrostatic residual stress (σ) in around weld-joint of ZrNbMoGe alloy is compressive stress which has minimum value at about -2.73 GPa in weldcore region.

INTRODUCTION

Zirconium alloys known as zircalloy-2 and zircalloy-4 are commercial metals with excellent corrosion resistance, good mechanical properties, very low thermal neutron cross section [1]. Those alloys have been predominantly used as fuel cladding in Boiling Water Reactors (BWR) and Pressurized (heavy) Water Reactors (PWR/PHWR). However, those alloys are very expensive and must be imported; therefore, there have been many research activities to find an alternative material for fuel cladding. Various other zirconium alloys can also be manufactured by using standard fabrication techniques. Research on the synthesis of zirconium alloys [2], adding the minor element of Mo, Nb and Ge, has been performed at the PTBIN-BATAN using a single-arc furnace for melting the compounds. It is found that the ZrNbMoGe alloys have very high hardness and strength; however, they are brittle and difficult to be rolled when they were fabricated. The new alloy has been further researched in the institution, funded by the Indonesian ministry of research and technology. Investigations have been carried out including analyzing the alloys by observing crystal structures [3] and microstructures using XRD and Scanning Electron Microscope respectively.

Recently, the effects of welding around weld-joints have been inspected to obtain information regarding stress behavior in three regions, i.e., weldcore, heat-affected zone, and base metal, by means of X-ray diffraction technique. These regions near the weld line undergo severe thermal cycles due to the intense concentration of heat in the heat source of welding. Thermal cycles cause non-uniform heating and cooling in the material, thus generating inhomogeneous plastic deformation and residual stresses in the weldments. The presence of residual stresses can be detrimental to the performance of welded product. Tensile residual stresses are generally detrimental, increasing the susceptibility of a weld to fatigue damage, stress

* Corresponding author.
E-mail address: farihin@batan.go.id

corrosion cracking, and fracture. Also, a residual stress may be created during the manufacturing process of a material, or it may accumulate in a structure over many years in operation. In either case, such a stress can adversely affect a product's quality, durability and lifetime. Accurate detection of residual stress is an important element of the quality control process and helps predict the service lifetime of products [4]. Residual stresses, both on exceptionally strained points and on the surfaces of moving parts, are routinely determined by XRD [4]. X-ray diffraction (XRD) is presently used to non-destructively measure residual stress. In addition, XRD allows non-contact measurements with unsurpassed spatial resolution and the ability to measure hardened materials. One way to perform residual stress measurements is by obtaining the whole pattern of diffraction data which is usually accompanied by the use of software implementing the Rietveld refinement method or also simply known as the Rietveld method.

The Rietveld method is capable of handling diffraction data obtained from X-ray diffractometers [5]. In the Rietveld method, the least square refinements are carried out until the best fit is obtained between the entire observed (powder) diffraction pattern taken as a whole and the entire calculated pattern based on the simultaneously refined models. Optical effects, instrumental factors, background and other specimen characteristics (e.g. lattice parameters) as may be desired, and the peak shape of patterns can be modelled. A key feature is the feedback, during refinement, between improving knowledge of structure and improving allocation of observed intensity to partially overlapping individual Bragg reflections.

The aim of this research is to investigate the presence of intergranular residual stresses in ZrNbMoGe alloys which are utilized as a cladding material after the welding process has been applied, by means of tailoring X-ray diffraction and Rietveld refinements method. Our observation was concentrated in three main regions, i.e., the weldcore, the heat-affected zone (HAZ), and the base metal.

THEORY

The strains and stresses discussed in this section are the average values over the entire irradiated volume. The residual stresses in most solid aggregates are, however, far from homogeneous. The presence of an inhomogeneous strain field results in a broadening in the diffraction profile. In general, peak broadening can be ascribed to either small particle sizes, an inhomogeneous strain field, or both. Typically, the broadening due to small particle size appears in the form of a Lorentzian function, whereas that due to the strain is described by a Gaussian function. The broadening of a diffraction peak due to the presence of an inhomogeneous [6] strain field is given by:

$$B^2 = B_O^2 + 32\ln 2\, e_{hkl}^2 \tan^2\theta = U\tan^2\theta + V\tan\theta + W \quad (1)$$

where B is the FWHM of the broadened peak and B_0 is the instrument resolution which varies with θ according to the Cagliotti [7] equation,

$$B_o^2 = U_o\tan^2\theta + V_o\tan\theta + W_o \quad (2)$$

Since only a modest R factor was achieved in the refinement, it is impractical to model the anisotropic inhomogeneous strain field with the present experimental data. Here, a simpler approach is taken to obtain an estimate of $\bar{e}$, the *average* value of the anisotropic *rms* strains within the specimens. Substituting equation (2) into equation (1), it can be obtained,

$$U = U_O + 32\ln 2\, e_{hkl}^2 \quad (3)$$

Equation (3) indicates that $\bar{e}$ can be estimated from the refined peak shape parameter U. In the calculations, the parameter U_0 was taken from the refinement of the base metal. Now that the lattice strains have been characterized, the residual stress in each phase can be deduced. Since no pressure was applied during the experiment, the residual stresses in each phase are expected to be hydrostatic. In fact, the average lattice strains discussed above, which were obtained from the refinement of a diffraction pattern over a wide angular range and hence represented some kind of average over many directions in the diffraction plane, are better measures of the hydrostatic stresses rather than the stresses along any particular specimen orientation. The hydrostatic stress, σ, is related to the hydrostatic [8] strain, $\bar{\varepsilon}$, by the following equation:

$$\sigma = \frac{\mathrm{E}}{1-2\upsilon}\bar{\varepsilon} \quad (4)$$

where E is Young's modulus and ν is Poisson's ratio of the specific material considered. The given parameters [9] for zirconium alloy are 99.3 GPa and

0.37, respectively. For a hydrostatic stress state, $\bar{\varepsilon}$ can be calculated along any direction with respect to the specimen orientation by $\bar{\varepsilon} = (1/4\pi) \int_{\Omega} \varepsilon_{hkl}\, d\Omega$, where ε_{hkl} is the strain within the grain whose [*hkl*] lies in the direction under consideration and the integration is performed over randomly oriented grains. It is shown that for orthorhombic phase the equation is:

$$\bar{\varepsilon} = \frac{1}{3}\left[\varepsilon_a + \varepsilon_b + \varepsilon_c\right] \quad (5)$$

For hexagonal and tetragonal phase, that equation becomes,

$$\bar{\varepsilon} = \frac{1}{3}\left[2\,\varepsilon_a + \varepsilon_c\right] \quad (6)$$

where ε_a, ε_b and ε_c are the strains in the direction of *a*-, *b*- and *c*-axis respectively. But the calculation for the strain of cubic phase the second order becomes ε_a and the average value is, hence, similar to the lattice strain itself. The residual stresses in the phases are not independent. Rather, they are governed by the equation of equilibrium [8],

$$f_o\sigma_o + f_c\sigma_c + f_h\sigma_h + f_t\sigma_t = 0 \quad (7)$$

where f_o, f_c, f_h and f_t are the volume fractions of orthorhombic, cubic, hexagonal and tetragonal phase, respectively. Equation (7) can be used to check whether the hydrostatic assumption is valid.

EXPERIMENTAL METHODS

The synthesis of the zirconium alloy was carried out by melting the elements of zirconium (Zr sponge), niobium (Nb), molybdenum (Mo) and germanium (Ge), using a single arc melting furnace in an argon atmosphere at a temperature higher than 1850°C. The weight percentage of the elements of the ingots being made was 97.5% Zr, 1.0% Mo, 1.0%Nb and 0.5% Ge, as indicated in Table 1. All of these elements were melted into the copper crucible which is equipped with a water coolant. By using tungsten electrode, with argon capacity of 5 liters/minute and electric current of 150 amperes, the elements were heated and melted. Afterward, the ingots were directly cooled in atmospheric condition to obtain zirconium alloy. Fig. 1 illustrates the experimental stages used in materials fabrication; (a) raw materials, (b) single arc melting furnace and (c) the ZrNbMoGe ingot.

Table 1. Chemical composition of the specimen.

Specimen	Composition of the elements (%wt)			
	Zr	Nb	Mo	Ge
Weld-ZrNbMoGe	97.50	1.00	1.00	0.50

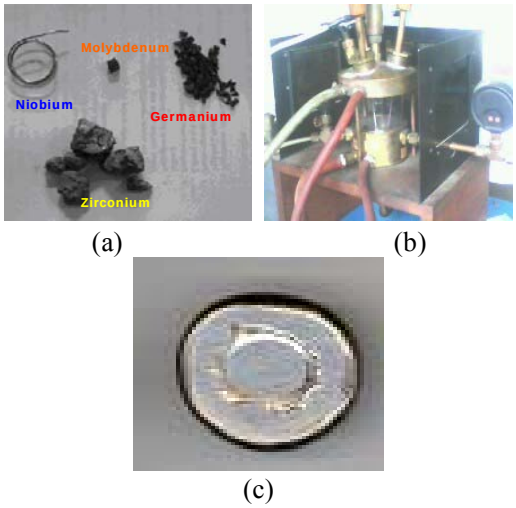

Fig. 1. (a) raw materials, (b) single arc melting furnace, and (c) ZrNbMoGe ingot.

In the hot-rolling process, the ingots were heated in the furnace until their temperature reached 850, 900 and 1000°C. At those points, they were rolled mechanically. The process was carried out in several steps with reduction rate of 5% per pass. This work was performed by using the hot rolling machine in the metalurgical laboratory of ITB Bandung. Fig. 2 ilustrates the hot rolling process of the specimen.

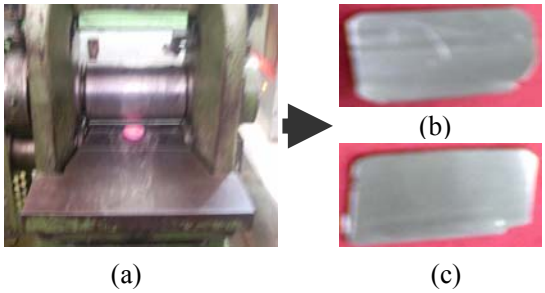

Fig. 2. Hot-rolling process of ZrNbMoGe plate; (a) rolling machine and (b-c) rolled plate.

Two parts of the plate specimens which had been rolled at temperature 850°C were then welded in BATAN Technology by using the TIG method with a current of 20 amperes, a voltage of 9.5 volts, and a weld-movement of 2 cm/minute. Fig. 3 sketches the welding process within position

of specimen, arc and butt joint. First, 4 mm-thick plates were formed into butt joint with a slope of 20° for stacking weld-system by adopting the zircalloy welding technique. Then, the specimen was prepared by grinding, light-polishing, alcohol etching, and ultrasonic cleaning.

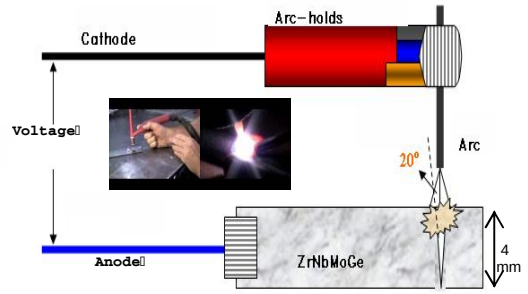

Fig. 3. TIG-welding process and scheme.

The macrostructure around weld-joint specimens was pictured by optical microscope with magnification of 50 times, while the microstructure of around the joint was observed by utilizing SEM-EDS with a magnification of 1000 times after the mounting, grinding, polishing and etching process.

Figure 4 shows the three symmetrical positions of diffraction scanning beams in a specimen, i.e., the weldcore, the HAZ and the base metal. The specimen was characterized using an X-ray diffractometer (XD-610) located in the PTBIN BATAN. The instrument was set on a Cu target which scatters a wave length of about 1.540 Å with instrument resolution of 0.02° in silicon (Si) standard. The X-ray diffraction patterns were scanned in the range of θ–2θ geometry to obtain a good peak to background ratio. Measurements were carried out by step counting mode of 0.05° and 2θ ranging from 30° to 75°.

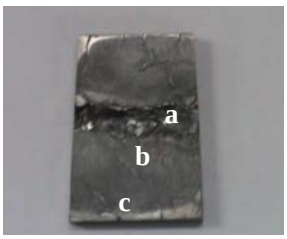

Fig. 4. Three position beam shoot of X-ray diffraction: (a) weldcore, (b) HAZ and (c) base metal.

RESULTS AND DISCUSSION

The microstructures around a weld-joint are shown in Fig. 5. Grains granulation in weldcore, HAZ and base metal regions are different from each another. The base metal region contains a mix of small and large grain sizes. The grain sizes appear similar and uniform in HAZ region, while the dendritic structures sphread out on surface of weldcore region. Fig. 5a shows that the welding is not good enough. It is seen clearly that some cavities and pores emerged into the surface. Many in-fusion phenomena occur along weld-joint line. In the weldcore region, the chemical composition data from EDS spectrum, listed in Table 2, show that Zr and Ge element contents are 79.24% and 0.67% respectively. The spectra can also be seen in Fig. 8, complete with numerical data of mass, atomic and error fraction of measurements. The data in Table 2 shows that Zr-Ge precipitate (Zr_3Ge and ZrGe) formation dominates the Zr-Mo precipitate ($ZrMo_2$) formation. It causes the structure and mechanical properties differ from other regions and may also affect the residual stress behavior in the material.

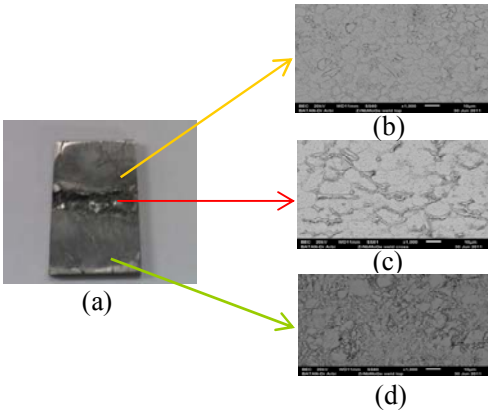

Fig. 5. (a) Macrostructure of welding specimen and micro-structures of: (b) heat-affected zone, HAZ, (c) weldcore and (d) base metal,(SEM; magnification of 1000 times).

Table 2. Mass fractions of Zr/Ge obtaining from EDS JEOL.

Element	Mass fraction (%wt.)		
	Base Metal	HAZ	Weldcore
Zr	71.24	73.13	79.24
Ge	2.24	-	0.67

In the other two regions, the precipitates of $ZrMo_2$ still have the same contribution to the grain boundaries. Granulation in the microstructure changes and grain growth in the weld region (weldcore) is smaller than that in the HAZ and in the base metal. Hardness measurements [10] performed on the specimen, around the weld-joint, produced the following hardness values: 214 VHN in the base metal, 221 VHN in the HAZ, and 240 VHN in the weldcore. A high hardness value in the weld region was probably due to the influence of natural quenching process, as in this case the region is heated during the process of welding and suddenly cooled after welding process. This process

allows the formation of stress-strain in the crystal grains with different orientations in three different regions (weldcore, HAZ and base metal). Judging from the picture above (Fig. 5a), the welding process is not acceptable for the fabrication of cladding. Improvements and further research activities are needed, especially in welding techniques which include sample preparation and seam formation, current selection, use of filler, and confinement of argon to prevent oxidation.

In Figs. 6a-c, the raw X-ray diffraction scanning data pattern and Rietveld refinement models are shown for the positions of the base metal, the HAZ, and the weldcore. In the figures there are signs or indications of line broadening, such as straight lines under both patterns (standard and model) which indicate the position of zirconium phase with a hexagonal crystal symmetry, while the phase position of $ZrMo_2$ (yellow line) exhibits a cubic crystal symmetry, Zr_3Ge (red pink line) exhibits tetragonal symmetry, and the ZrGe phase (black line) is orthorhombic. Fig. 6 shows the Rietveld refinement diffractogram of ZrNbMoGe alloy material around the weld-joint using a four-phase modeling analysis.

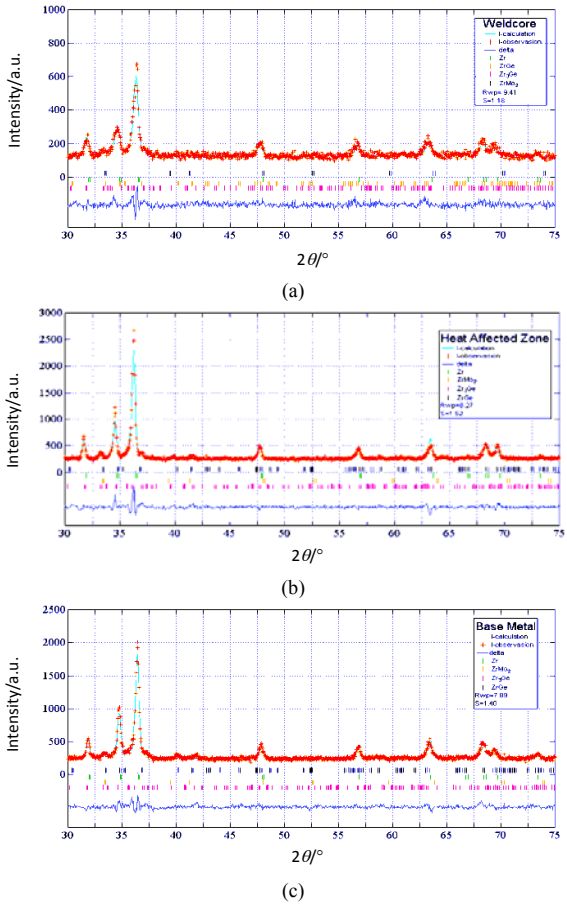

Fig. 6. Rietveld refinement profiles of ZrNbMoGe alloy in around weld-joint: (a) weldcore (b) HAZ and (c) base metal.

The refinement of the specimen was performed using a model that consists of four phases, namely zirconium (hexagonal) phase with space group *P63/mmc* (I-194), ZrGe phase (orthorhombic) with space group *Pnma* (I-62), Zr_3Ge phase (tetragonal) with a space group *P42 / n* (I-86) and the $ZrMo_2$ phase (cube) with space group *Im3m* (I-229) [11]. The peak shape profile of each phase is separately modeled using a pseudo-Voight function [12,13] which is a combination of Gaussian and Lorentzian linear function. The angular range of the experimental data is sufficient to allow the structural parameters of each phase to be refined. These structural parameters include lattice parameters, isotropic thermal parameters, zero deviation, anisotropic parameter (preferred orientation), and the profile parameters. The four-phase refinement model is quite satisfactory for each specimen, with the R_{wp} varying between 7% and 9% and the value of the reliability factor varying between 1.1 and 1.5, as shown in Fig. 6 and Table 3. The lattice parameters′ and peak profile refinements for the four phases in ZrNbMoGe alloys and single phase zirconium vary slightly from the base metal to weldcore. Positive value thermal parameters obtained from the refinement which has added to the validity and the reliability of the acquisitioned data. Figs. 6a-c show the refined structure patterns with a reduced display indicating that for this specimen the profile (model) closely matches the experimental data.

Table 3. Fraction of phase and reliability factor of welded specimen ZrNbMoGe alloy from Rietveld refinements.

Phase	Fraction of Phase (%)		
	Base Metal	HAZ	Weldcore
Zr	78.58	69.51	55.64
Zr_3Ge	12.54	22.13	28.68
$ZrMo_2$	2.39	7.01	2.74
ZrGe	6.49	1.35	12.94
Refinements Parameter			
Rwp (%)	7.89	8.27	9.41
$S_{(reliability\ factor)}$	1.40	1.52	1.18

The fractional values contained in the ZrNbMoGe alloy weld specimens with the elemental composition of 0.5 wt% Ge are tabulated in Table 3. The values are calculated from the ratio of the intensity of the diffraction peaks and are normalized to the highest intensity contained in the diffraction pattern. According to the equation $W_m = (SZV)_m / \Sigma_i S_i Z_i V_i$ [14], the value of the mass fraction of each grown crystal in a material can be obtained simply by entering the parameter scale factor *S*, number of molecules *Z*, the molecular weight *M* and the unit cell volume *V*. The RIETAN program automatically calculates the mass fraction

simultaneously throughout the crystal phase materials. Based on the calculation results tabulated in the table, for the angular range between $2\theta = 35°$ and $2\theta = 75°$, in the three regions of base metal, HAZ and weldcore, the mass fractions are highly variable. The base metal region tends to have the same pattern as the weldcore region, in accordance with the laws of Gibbs energy thermodynamics since the formation activation energy of Zr-Ge precipitates is lower than the formation activation energy of Zr-Mo precipitates.

The result of the calculation shows that for all three regions (base metal, HAZ and weldcore), the zirconium phase is very dominant in this material with a fractional amount of 78.58%, 69.51% and 55.64% respectively. Meanwhile the Zr_3Ge phase fraction gradually increases, first to 12.54%, followed by 22.13% and 28.68% in the successive region of the base metal, HAZ and weldcore. The quantitative behavioral pattern of this phase is graphically presented in Fig. 7.

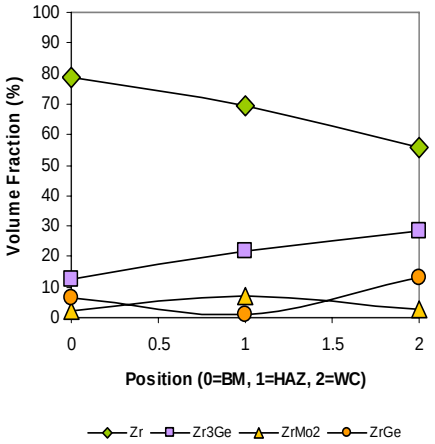

Fig. 7. Fraction of phases in welded specimen of ZrNbMoGe alloy from Rietveld refinements.

Meanwhile, there is an interesting phenomenon in the HAZ. Compared to the other two regions (base metal and weldcore), this region aberrantly exhibits the maximum value of the $ZrMo_2$ phase at 7.01%, whereas the ZrGe phase reaches the lowest minimum value of 1.35%. The phenomenon could be explained using the EDS observation results shown in Fig. 8 and compiled in Table 2 which shows that 73.13% of the HAZ area consists of the element Zr, but no elemental Ge was detected in the spectrum; the elemental Ge may have evaporated becauseit is so volatile. This leads to the minimum formation of Zr-Ge (ZrGe) precipitates when compared to Zr-Mo ($ZrMo_2$), although according to materials thermodynamics, the Gibbs free energy of Zr-Ge formation is lower than that of Zr-Mo.

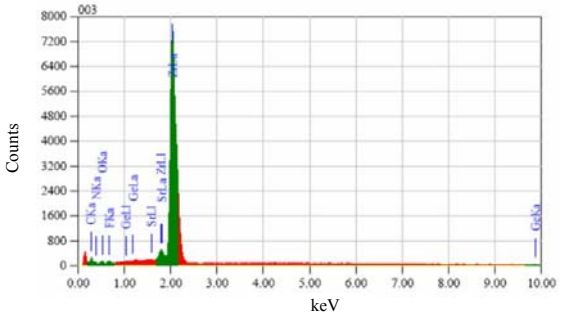

Element	(keV)	Mass%	Error%	Atom%	K
C K	0.277	11.18	0.40	40.06	1.3212
N K*	0.392	2.95	1.43	9.06	1.7691
O K	0.525	3.61	0.65	9.72	1.4549
F K	0.677	1.26	0.35	2.85	0.3263
Ge K	9.874	0.67	1.84	0.40	0.8345
Sr L*	1.806	1.08	0.31	0.53	1.5103
Zr L	2.042	79.24	0.33	37.38	92.8738
Total		100.00		100.00	

(a)

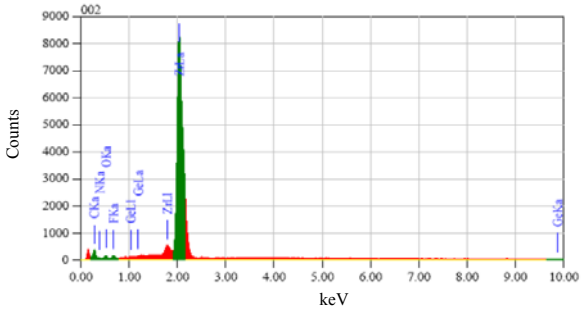

Element	(keV)	Mass%	Error%	Atom%	K
C K	0.277	16.50	0.33	48.26	2.0090
N K*	0.392	4.31	1.30	10.80	2.5765
O K	0.525	4.52	0.58	9.93	1.8422
F K*	0.677	1.54	0.31	2.85	0.4076
Ge K					
Sr L*					
Zr L	2.042	73.13	0.28	28.16	93.1647
Total		100.00		100.00	

(b)

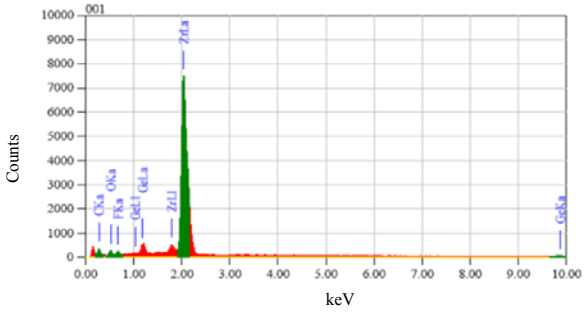

Element	(keV)	Mass%	Error%	Atom%	K
C K	0.277	16.29	0.34	48.74	2.0406
N K*					
O K	0.525	7.67	0.55	17.22	3.4961
F K	0.677	2.57	0.32	4.85	0.7083
Ge K	9.874	2.24	1.63	1.11	2.9936
Sr L*					
Zr L*	2.042	71.24	0.29	28.07	90.7615
Total		100.00		100.00	

(c)

Fig. 8. Mass fraction of the element from *Energy Dispersive Scanning* (EDS) in welded specimen of ZrNbMoGe alloy: (a) weldcore (b) HAZ and (c) base metal.

The phenomenon of residual stress in the material can simply be predicted from the measured crystal lattice's strain, namely the shift of the diffraction plane peak as observed in the diffraction pattern, whereas the tensile strength of the crystal field or strain field can be calculated from the observed diffraction peak broadening. Fig. 9 shows the shift and broadening pattern of the ZrNbMoGe alloy (10$\bar{1}$0), (0002) and (10$\bar{1}$1) plane diffraction peaks. The values of the angular peak shifts and peak broadening for the three diffraction planes obtained by neutron diffraction method are tabulated in Table 4.

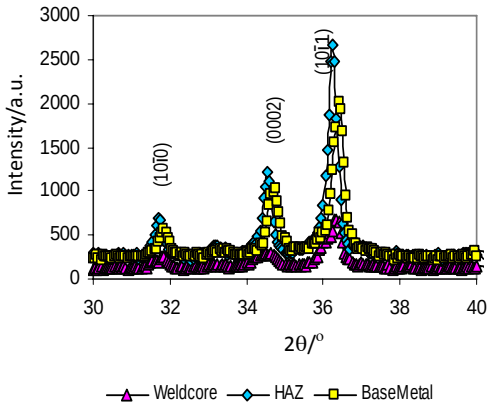

Fig. 9. Shifting and broadening of diffraction peak in welded specimen of ZrNbMoGe alloy.

Table 4. Shifting and broadening of three Bragg's planes of zirconium phase.

Specimen	Shifting 2θ (deg.)			Broadening FWHM (deg.)		
	(10$\bar{1}$0)	(0002)	(10$\bar{1}$1)	(10$\bar{1}$0)	(0002)	(10$\bar{1}$1)
Base Metal *(reference)*	31.932	34.788	36.487	0.415(5)	0.417(6)	0.419(0)
HAZ	31.885	34.719	36.429	0.262(5)	0.264(5)	0.260(0)
Weldcore	31.934	34.800	36.492	0.315(0)	0.343(5)	0.331(8)

The values of peak shifting and broadening for the three regions vary considerably, but sufficient to provide information on the changes in the dynamics of the specimen's crystal lattice. The phenomenon of peak broadening can be attributed to the small particle sizes, or the inhomogeneous strain field, or both. A broadening due to smallness of particle size appears in the form of Lorentzian functions, whereas a broadening due to strains is described by a Gaussian function. Fig. 9 demonstrates that the diffraction peaks can be well modeled by a Gaussian function. The Rietveld analysis of the measured diffraction patterns reveals only a small Lorentzian component in the peak shape profile. Thus the observed widespread broadening in the ZrNbMoGe alloy specimens is due to the inhomogeneous strain field rather than to the particle size. It could be observed from the diffraction peak profile that there are differences in the widths of the curves, and the differences represent anisotropic peak broadening. The origin of the anisotropic strain varies. The presence of defects along a particular [*hkl*] direction shows spatial fluctuations with respect to the d_{hkl} in the grain, and causes a broadening in the (*hkl*) reflection. The variation of d_{hkl} from grain to grain also contributes to the broadening of the (*hkl*) plane. There is an impression that the inhomogeneous strain field in the zirconium matrix is caused by an inclusion of zirconium particles (minor phase). Halmos [15] reported that the anisotropic strain broadening is caused by the concentration of dislocations associated with the close-packed plane.

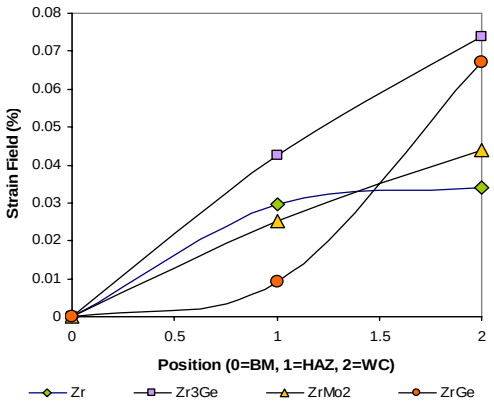

Fig. 10. Strain field of the phases in welded specimen ZrNbMoGe alloy.

The presence of an inhomogeneous strain field produces a broadening in the diffraction profile, therefore the residual stress in most solid aggregates is very far from homogeneous. All observed regions in the zirconium alloy specimens in this experiment showed some degree of peak broadening, as indicated in Fig. 10, where the points are obtained from the X-ray diffraction measurements with Gaussian models. The actual value of the strain field is not negative because it is in the quadratic equation (absolute value). In regression analysis, the strain field lines are entirely above the x-axis. The minor phases were having an increasingly stronger strain, whereas in the zirconium phase the strain is becoming less prominent with the line becoming more level, as it stretches from the HAZ to the weldcore. This phenomenon gives rise to the hypothesis that the minor phase is growing, where the dopant atoms are able to bind and dislocate the atomic matrix (zirconium). Meanwhile, the region around the HAZ and the weldcore, strain field lines for the three phases ,namely Zr, $ZrMo_2$, and ZrGe intersect each other, which supports the assumption that in the

intersection the specimens′ strain is homogeneous (isotropic). The three phases (Zr, ZrGe, and $ZrMo_2$) are having isotropic strain around the transition region from the HAZ to the weldcore.

The lattice parameters of each phase calculated by the RIETAN program are tabulated in Table 5. In line with the theoretical basis that the interplanar distances is directly proportional to the lattice parameters, equations (2) and (3) can be used to calculate the average lattice strain along certain crystallographic directions, where d and d_0 are successively replaced by a and a_0, b and b_0 or c and c_0. Lattices a, b and c are the materials′ strained lattice spacing, and lattice constants a_0, b_0 and c_0 is the stress-free lattice spacing (reference). In this case the strain tensor is adapted to the crystal symmetry. The number of free components can be reduced to one, two or three independent components. In a uniaxial crystal structure, such as the cubic structure, only one free component is required, whereas for the hexagonal/tetragonal structure only two independent components are needed, and for the orthorhombic structure three free components are necessary in order to completely represent the properties of the tensor [16]. Along the other directions, the strains can be calculated using the principles of tensor algebra. It is highly recommended to determine the components of the strain along the direction of the principal axes, which are the a-axis in the $ZrMo_2$-phase, a- and c-axes for the Zr and Zr_3Ge-phase and the a-, b- and c-axes for ZrGe phase following the rules of conventional structure.

Table 5. Lattice parameter in welded specimen of ZrNbMoGe alloy from Rietveld refinements.

Phase	Lattice Parameter (Å)								
	Base Metal			HAZ			Weldcore		
	a	*b*	*c*	*a*	*b*	*c*	*a*	*b*	*c*
Zr	3.2333(4)	3.2333(4)	5.1517(4)	3.2382(0)	3.2382(0)	5.1632(6)	3.2335(6)	3.2335(6)	5.1533(5)
$ZrMo_2$	7.5912(1)	7.5912(1)	7.5912(1)	7.5726(4)	7.5726(4)	7.5726(4)	7.5920(9)	7.5920(9)	7.5920(9)
Zr_3Ge	11.3259(8)	11.3259(8)	5.2505(1)	11.2600(1)	11.2600(1)	5.3176(6)	11.2903(5)	11.2903(5)	5.2789(7)
ZrGe	8.2338(6)	4.2112(4)	5.3370(7)	8.1752(7)	4.4976(3)	5.3395(1)	8.2338(9)	4.2124(2)	5.3536(4)

The residual stress in each phase can be deduced from the characterization and analysis of the lattice strain. During the experiment, there was no applied pressure; therefore, the residual stress in each phase is considered hydrostatic. The average lattice strain discussed above is obtained from the refinement of the diffraction pattern for the entire angular range of 2θ. The strain represents average value in some direction in the diffraction plane. This type of hydrostatic strain measurement is more precise than the stress measured along the particular direction of a specimen. The hydrostatic tension σ is calculated using equation (1). In this condition, the average strain ε estimated along the direction of the reference orientation of the specimen is calculated by equation (2) and (3). The parameters E and ν used in the calculation of σ, are obtained from a separate mechanical measurements reported in the literature [9]. For zircalloy material at room temperature, these mechanical parameters are 99.3 GPa and 0.37 respectively. Fig. 11 shows the hydrostatic stress which is calculated as a function of the position of point diffraction measurements (three measurement regions: the base metal, the HAZ and the weldcore). Identically to the behaviour of the lattice strain, the calculated hydrostatic stress in the ZrGe minor phase is a tensile stress for all the measurement regions, while in the zirconium matrix it is always tensile. On the other hand, the calculated hydrostatic stress in the $ZrMo_2$ minor phase is compressive in the HAZ region and tensile in the weldcore regions, while the minor phase Zr_3Ge is experiencing a significant compressive pressure in all regions of measurement.

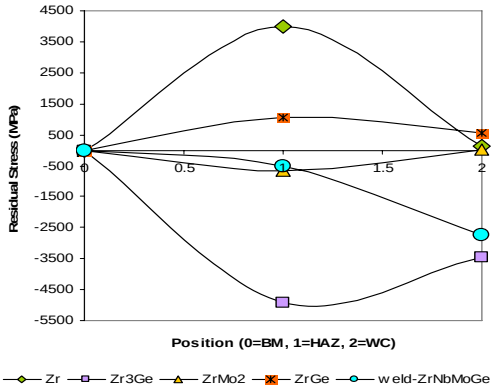

Fig. 11. Hydrostatic residual stress distribution in welded specimen of ZrNbMoGe alloy.

In the HAZ, the magnitudes of the tensile stress in the Zr and ZrGe phase are approximately 3.99 GPa and 1.05 GPa respectively, whereas in the Zr_3Ge and $ZrMo_2$ phase the compressive stress is about -4.92 GPa and -0.65 GPa respectively. The total residual stress contained in the region is -0.53 GPa. When measurements are shifted to the weldcore region, hydrostatic tensile stress calculated in the Zr and ZrGe phase tend to fall in the range of 0.14 GPa to 0.56 GPa, while the $ZrMo_2$ phase reversed direction and experience a tensile stress of 0.01 GPa, and the compressive residual stress in the Zr_3Ge phase increases to -3.45 GPa. The dominance of the Zr_3Ge phase was such that it causes the total residual stress in the weldcore of ZrNbMoGe alloys to experience a sharp decline toward the compressive stress of -2.73 GPa. The curves show

that in all regions of measurement, the residual stress of the weld specimen is controlled by the compressive residual stress of the minor Zr_3Ge phase. This conclusion is supported by the fact that the residual stresses in the matrix Zr and in the minor phases are not independent but linked together in an equilibrium relationship [8].

From the behavior pattern of the curve, it is very logical to assume the hydrostatic stress in the weld specimen is caused by the presence of Zr_3Ge particles which shift the dominance of the Zr matrix. This finding is consistent with the strain field data shown in Fig. 10. The minor strain field phase increased significantly, while the strain field Zr phase increased slowly and even tends to be flat.

Also, as shown in Fig. 12, the behavior of the curve resulting from this research conforms with the results of other residual stress measurements in low carbon steel weld pads on the root side of welding specimen after different weld passes as reported by Murugan et.al. [17]. Fig. 12 compares the residual stress data within both welding specimens, i.e., low carbon steel weld pads and weld-ZrNbMoGe alloy. The residual stresses in both welding specimen tend to gradually decrease in magnitude and even sharply decline in the direction from the HAZ to the weldcore in the weld-ZrNbMoGe specimen.

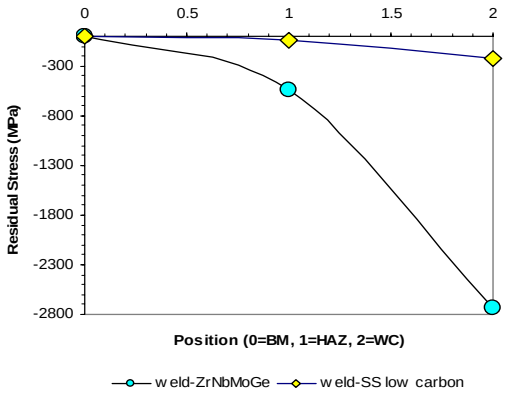

Fig. 12. Comparison of residual stress distribution in weld-ZrNbMoGe and SS low carbon.

CONCLUSION

It can be concluded that: grains granulation around the weld shows three different regions: the weldcore (dendritic; cast structure), the HAZ (medium grain and uniform), and the base metal (large and small grains). The four-phase Rietveld refinement model was satisfactory for each specimen, with the R_{wp} varying between 7% and 9% and the value of the trust factor (reliability factor) varying between 1.1 and 1.5. Refined structural patterns with a profile display (model) that indicate a reduction, closely match the experimental data for the specimen. The fraction of the minor phase in the material tends to increase only in the HAZ; the phase of ZrGe is smaller than the $ZrMo_2$ phase caused by of evaporation the Ge (volatile) element in the region. The phenomenon of residual stress in the material can simply be predicted from the observed crystal lattice strain, namely the shift of the peak regions of the diffraction pattern. The tensile strength of the crystal plane and the strain field can be calculated from the observed diffraction peak broadening. The hydrostatic residual stress behavior of materials shows the predominance of the $ZrMo_2$ and Zr_3Ge minor phases in the Zr matrix. The minor phase is observed to have a severe strain, whereas the zirconium phase is having a weaker strain, with the lines sloping from the HAZ to the weldcore region. The hydrostatic residual stress (σ) around the weld-joint in the ZrNbMoGe alloy material with the composition of 97.5%Zr1%Nb1%Ge0.5%Mo is a compressive residual stress which reaches a minimum value of -2.73 GPa in the weldcore region.

ACKNOWLEDGMENT

The writers would like to express their thanks to Drs. Gunawan, M.Si., Dr. Sudaryanto,M.Eng., Ir. Djoko Hadi Prayitno, M.Eng., Drs. Bambang Sugeng, M.T. for their kindness and help. Also, the writers would like to express special thanks to Dr. Azis Khan Jahja, M.Sc. and Prof. Dr. Rer.Nat. Evvy Kartini, for their helpful discussions.

REFERENCES

1. J. R. Lamarsh, Introduction to Nuclear Engineering, Addison–Wesley Publ. Co., New York (1983) 644.
2. A.H. Ismoyo, Parikin and B. Bandriyana, Indonesian Journal of Materials Science **10** (2009) 199. (in Indonesian).
3. Parikin, A.H. Ismoyo and B. Bandriyana, Scientific Magazine of Industrial Assesments **5** (2011) 305. (in Indonesian).
4. http://www.rigaku.com/applications/residual_stress_analysis. Retrieved in October (2012).
5. A.C. Larson and R.B. Von Dreele, General Structure Analysis System, the Regents of the University of California, Los Alamos, New Mexico (1994) 1.

6. H.P. Klug and L.E. Alexander, X-ray Diffraction Procedures, 2nd ed., Willey, New York (1974) 618.

7. G. Cagliotti, A. Paoletti and F.P. Ricci, Nucl. Instrum. **3** (1958) 223.

8. I.C. Noyan and J.B. Cohen, Residual Stress Measurement by Diffraction and Interpretation, Springer-Verlaag, New York (1987) 1.

9. Anonymous, Reactor Grade Zirconium Alloys for Nuclear Waste Disposal. http:// alleghenytechnologies.com/wahchang. Retrieved in October (2012).

10. B. Bandriyana, A.H. Ismoyo and Parikin, *Change of Hardness and Microstructure due to the Rolling and Welding Process of the Zr-Nb Mo-Ge Alloy Used for NPP Cladding Materials,* Proceedings of The National Conference of Scientific Presentations and Meeting Basic Research and Science and Nuclear Technology (2012) 70. (in Indonesian).

11. P. Villars and L.D. Calvert, Pearson's Handbook of Crystallographic Data for Intermetallic Phases, 2nd edition, ASM International, New York **3** (1991) 3824.

12. R.A. Young, The Rietveld Method, IUCr Book Series 5, International Union of Crystallography, Oxford University Press, UK (1997).

13. H.M. Rietveld, J. Appl. Crystallogr. **2** (1969) 65.

14. R.J. Hill and C.J. Howard, J. Appl. Crystallogr. **20** (1987) 467.

15. G.T. Halmos, High Production Roll Forming, SME, Michigan (1983) 1.

16. J.F. Nye, Physical Properties of Crystals, Oxford University Press, Oxford, UK (1985) 1.

17. S. Murugan, S.K. Rai, P.V. Kumar, T. Jayakumar, B. Raj and M.S.C. Bose, Int. Journal of Pressure Vessels and Piping **78** (2001) 307.